LBNL–54918
HIFAN 1320

Initiation of long, free-standing z-discharges by CO_2 laser gas heating

C. Niemann*, A. Tauschwitz, D. Penache, S. Neff, R. Knobloch, R. Birkner, R. Presura†, D.H.H. Hoffmann
Technische Universitaet Darmstadt, Schlossgartenstr. 9, 64289 Darmstadt, Germany

S.S. Yu, W.M. Sharp
Lawrence Berkeley National Laboratory, 1 Cyclotron Road, Berkeley, CA 94720, USA

High current discharge channels can neutralize both current and space charge of very intense ion beams. Therefore they are considered as an interesting alternative for the final focus and beam transport in a heavy ion beam fusion reactor. At the GSI accelerator facility, 50 cm long, stable, free-standing discharge channels with currents in excess of 40 kA in 2 to 25 mbar ammonia (NH_3) gas are investigated for heavy ion beam transport studies. The discharges are initiated by a CO_2 laser pulse along the channel axis before the discharge is triggered. Resonant absorption of the laser, tuned to the ν_2 vibration of the ammonia molecule, causes strong gas heating. Subsequent expansion and rarefaction of the gas prepare the conditions for a stable discharge to fullfill the requirements for ion beam transport. This paper describes the laser-gas interaction and the discharge initiation mechanism. We report on the channel stability and evolution, measured by fast shutter and streak imaging techniques. The rarefaction of the laser heated gas is studied by means of a hydrocode simulation.

PACS numbers: 52.80.Tn, 52.58.Hm, 41.85.Ja, 42.62.-b

I. INTRODUCTION

High current discharge channels have been investigated for a number of years as the mainline final focus scenario for light ion beam fusion [1–3]. Ballistic transport of light ion beams inside the chamber of an inertial confinement fusion reactor was impossible due to the high space charge of the intense ion beams. A sufficiently dense plasma can neutralize both beam space charge and current of such beams, making channel transport relatively insensitive to details of beam current, pulse shape and emittance. First experiments, based on wall stabilized [4,5] and wire initiated [6,7] discharges demonstrated efficient ion beam transport over several meters. However, in a repetitively operated fusion reactor guiding structures like insulators and wires inside the reactor chamber can not be used since they are destroyed in every micro explosion.

Recently plasma channel transport was revived as an alternative for the final focus in heavy ion beam fusion [8,9]. As a first step experiments in Berkeley [10] as well as at GSI [11] have been started. In both cases the discharges are initiated in metallic chambers. For this reason laser guiding of the channels is indispensable to prevent breakdown along the wall and to produce a discharge channel. Both experiments differ in the laser-gas combination and the initiation mechanism but have very similar discharge parameters. While in the Berkeley experiment the discharge is guided by an UV-laser pulse creating a seed of electrons in a gas fill of organic molecules, in the GSI experiment the gas along the channel axis is heated by an infrared laser. This method was used first successfully by Olsen [2] at currents below 30 kA. Other possible laser-gas combinations are summarized in [8].

This paper describes the laser gas heating and channel initiation in the experiment at GSI. The channel stability and evolution are discussed to prepare the basis for the ion beam transport experiments and advanced channel diagnostics which will be reported in following papers.

II. EXPERIMENTAL SETUP

The GSI laser channel experiment consists of a cylindrical, stainless-steel discharge chamber of 50 cm length and 60 cm diameter with two high voltage electrodes on opposite sides, insulated from the chamber by plexiglas plates (figure 1). The chamber is filled with ammonia (NH_3) at pressures between 2 and 25 mbar in a steady gas flow. Before the discharge is triggered, a CO_2 laser pulse is fired into the chamber through a ZnSe entrance window and a 15 mm diameter bore hole in the anode. The laser beam leaves the chamber through a second ZnSe window in the cathode, where the energy is measured by a pyroelectric detector. With a wavelength tuned to a molecular vibration of the NH_3 molecule, laser energy is efficiently coupled into the gas. This heating causes an expansion of the gas, creating a rarefaction channel along the desired path of breakdown on the chamber axis surrounded by a stabilizing gas wall.

*Electronic mail: C.Niemann@gsi.de
†present address: University of Nevada, Reno, NV 89557, USA

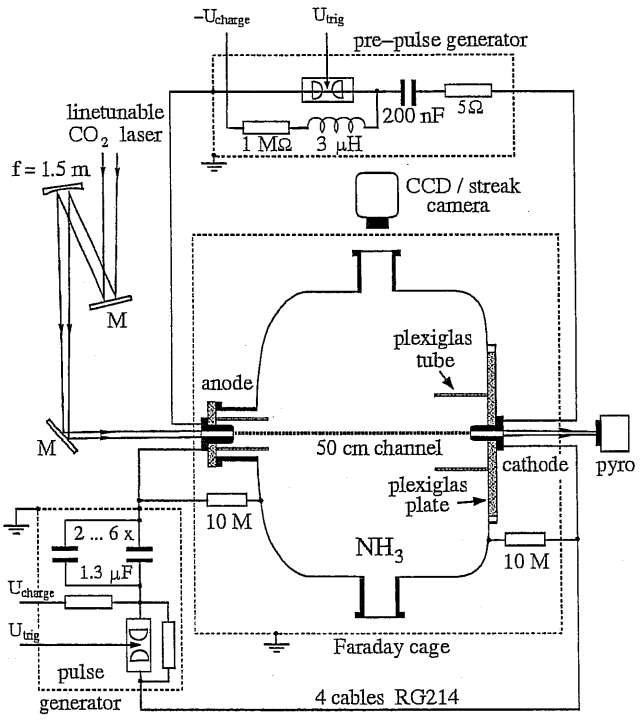

FIG. 1. Setup of the GSI laser channel experiment.

Some microseconds after the laser pulse, a capacitor bank of 2.6 to 7.8 μF charged to 20 kV is connected to the electrodes by a spark gap switch. To prevent breakdown from the electrodes directly to the chamber a plexiglas tube extends 10 cm into the chamber from each side. To further stabilize or shape the channel, a low energy prepulse discharge can be applied from a seperate pulse generator with a 200 nF capacitor in between the laser pulse and the main discharge. While the prepulse is optional, the laser pulse is crucial for a successfull channel creation. Without the laser pulse the discharge will always break down to the wall and so distinguishes this experiment from previous ones [12]. Both pulse generators as well as the discharge chamber are enclosed in Faraday cages with only small entrance ports for the laser and diagnostics. The chamber is kept on mid-potential between the electrodes by two 10 $M\Omega$ resistors. Both anode and cathode are stainless steel cylinders with diameters of 5 cm and 3 cm respectively. Four cables (RG 214) connect the main capacitor bank to the electrodes to keep the inductance low. The total circuit inductance and the resistance for a 2.6 μF capacitor, measured with a 60 cm long 1 cm diameter brass rod replacing the plasma channel is $815 \pm 1\ nH$ and $54 \pm 2\ m\Omega$ respectively. The current rise time for a discharge with a capacitor of 7.8 μF charged to 20 kV is around 4 μs depending on the pressure. A calibrated shunt measuring the total current driven by the pulse generator is used to determine the discharge current.

III. LASER-GAS INTERACTION

The CO_2 laser (SLCR TEA Model ML204) is linetuneable by a diffraction grating, giving around 5 J of energy in a single line in a 1 μs pulse. A f = 1.5 m concave mirror focuses the laser in the middle of the discharge chamber. The footprint of the rectangular beam profile varies only slightly from 0.9 cm^2 in the focus to 1.1 cm^2 near the electrodes. The maximum energy density in the chamber is around 2 J/cm^2. The 1.5 m focal length was a compromise between uniformity along the channel and energy density. The wavelength was adjusted to the P(32) transition for peak absorption, matching the $\nu_2 = 950\ cm^{-1}$ vibrational mode in NH_3 [12]. In this way a large fraction of the laser energy is absorbed as the beam passes through the 50 cm long gas filled chamber, down to pressures of a few mbar (figure 2). Compared to an untuned CO_2 laser oscillating at 10.6 μm the line tuning improves the absorption by more than one order of magnitude. The absorption A was measured with a pyroelectric detector behind the chamber. Since only one detector was available, several shots were averaged to compensate laser energy fluctuations, and compared with the energy measured behind the evacuated chamber. The bandwidth for resonance detuning is around 10 nm (FWHM) as determined from the decrease of absorption in 20 mbar from 90 percent down to almost zero. Changing the wavelength by a few nm around the resonance can adjust any absorption in between the extremes. The absorption cross section is calculated from the measured transmissivity $T = 1 - A$ by

$$\sigma = 1/(N \cdot L) ln(1/T) \qquad (1)$$

where N is the molecular density and L the length of the interaction volume. The absorption of the laser energy I along the gas cell is given by $\partial I/\partial z \sim -\sigma \cdot I$ assuming $\frac{1}{c}\partial I/\partial t \ll \partial I/\partial z$ which is the case for the short laser pulse length. This leads to an exponential decrease of energy deposition along the channel, causing an exponential temperature decay along the channel.

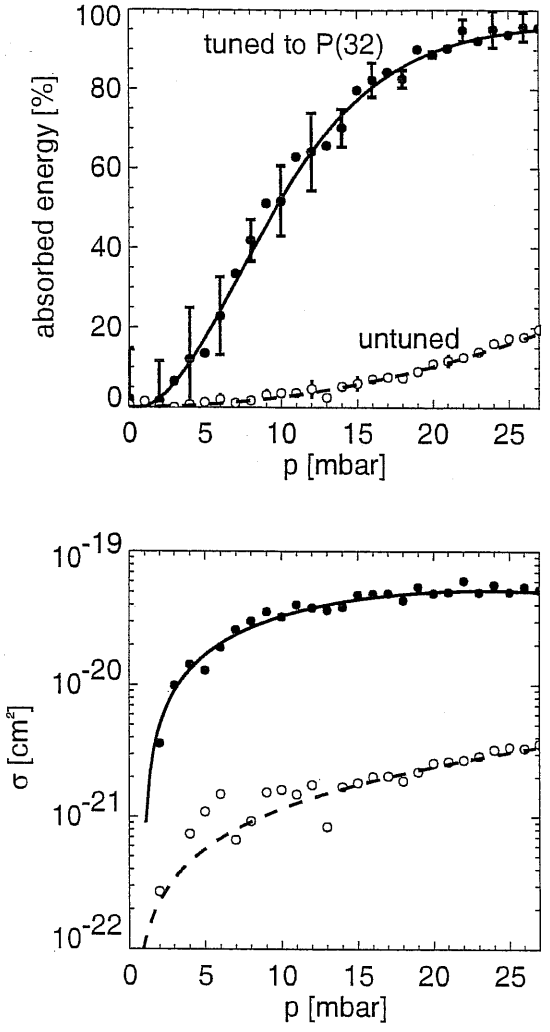

FIG. 2. Absorbed laser energy und absorption cross section as a function of pressure for an untuned laser oscillating at 10.6 μm as well as the laser tuned for peak absorption, both at 1.8 J/cm^2 incident laser energy. The error bars represent the standard deviation of three different laser shots.

The absorption does however also depend on the incident laser energy. Saturation effects in NH_3 lead to a decreased absorption cross section for a higher energy density. The saturation was measured in 4.5 and 10 mbar ammonia for an energy density ranging from 0.6 to 2.1 J/cm^2 (figure 3). The cross section varies by more than a factor of two for the 10 mbar gas fill. The temperature near the entrance is therefore slightly decreased compared to the exponential case. An absorption close to 100 percent is not favourable because of the strong temperature variation along the channel. Different gas expansion and rarefaction near cathode and anode lead then to unsymmetric initial conditions for the discharge. The saturation as well as the temperature dependence of the heat capacity of ammonia make an estimation of the laser gas heating effect rather complex. An interaction model was developed in [12] to calculate the temperature of the laser heated gas in longer gas cells, including saturation effects. For an energy density of 2.5 J/cm^2 temperatures changing almost linearly from 1500 K at the entrance down to 700 K near the exit of the chamber were calculated for a 26 mbar gas fill.

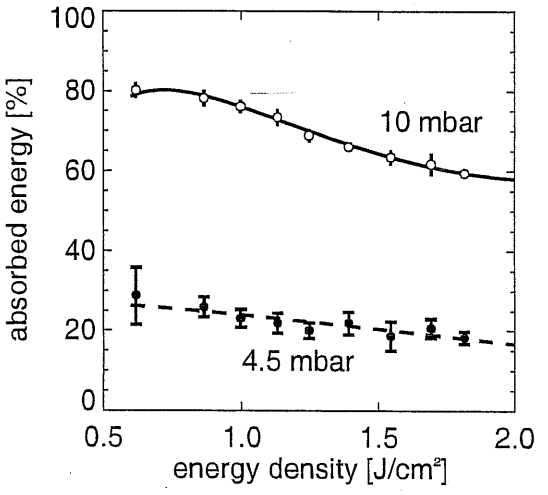

FIG. 3. Absorption as a function of incident laser energy density.

The same paper reports in detail on cross sections of other ammonia lines as well as resonance lines of different gases which are appropriate candidates for CO_2 laser heating. Ammonia was chosen for the experiment described in this paper, because of its small heat capacity, fast vibrational-translational relaxation time and because of the fact that NH_3 leaves no carbon deposits in the chamber after the discharge.

IV. CHANNEL INITIATION

The expansion of the heated gas and the creation of a rarefaction channel on the predefined discharge axis lead to a decrease in breakdown voltage and thus guide the discharge along the laser path, while the surrounding gas wall contributes to the stability of the discharge channel. According to [13] such a gas wall reduces the MHD instability growth rate by a factor of $(\rho_p/\rho_g)^{1/2}$, where ρ_g is the the ion density of the surrounding gas and ρ_p is the ion density of the pinch. The reduction of breakdown voltage due to the laser pulse is illustrated in figure 4. For the measurement the prepulse capacitor was charged step by step to higher voltages until a breakdown occured within 10 μs after the laser pulse was fired. The laser shows the biggest effect for a pressure of 15 mbar, reducing the breakdown voltage to 60 percent of the value for an insulator breakdown.

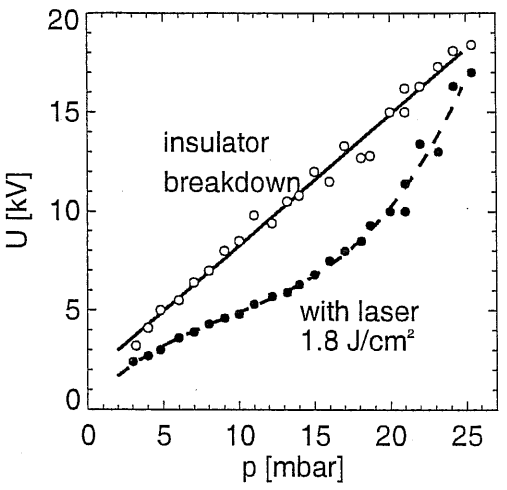

FIG. 4. Breakdown voltage as a function of pressure, with and without the laser pulse. Without laser pulse the breakdown occurs around the insulators and the current flows on the chamber wall.

At low pressures the absorption is too small to show a big effect while at higher pressures the entire laser energy is absorbed in the first few centimeters of the chamber so that no gas is heated near the cathode. However, self breakdown does not occur between the two electrodes directly but from the electrodes to the wall, which is possible at a lower threshold voltage. Therefore the laser decreases the gas breakdown voltage by more than 40 percent. A direct measurement in this experiment is not possible due to the metallic chamber. Olsen [17] measured a one and half fold reduction in breakdown voltage for an energy deposition of 2 J/cm^2 in an insulating ammonia gas cell. For 30 J/cm^2 the breakdown voltage was reduced by more than a factor of ten.
The breakdown voltage shows an almost linear decrease with incident laser energy density (figure 5).

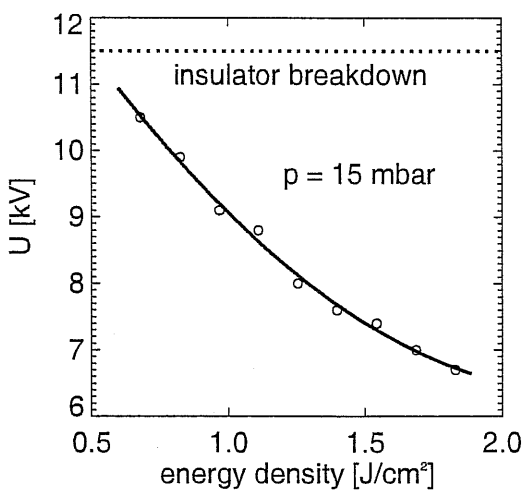

FIG. 5. Breakdown voltage for 15 mbar as a function of deposited laser energy.

A lower laser energy limit for a successfull channel creation is reached when the breakdown voltage becomes comparable to the voltage for insulator breakdown, in the case of a 15 mbar gas fill at an energy density of around 0.5 J/cm^2. If the voltage is higher than the voltage for insulator breakdown, the laser pulse will still produce channels. No upper limit could be measured in the accessible parameter range up to 20 kV. In this case it is possible to create channels with discharge trigger delays up to milliseconds.

The hydrodynamics of the laser heated gas was simulated by a one-dimensional Lagrangian fluid code CYCLOPS which was developed and used to model several aspects of the pinch experiments in Berkeley [14–16]. Figure 6 shows the evolution of the gas density during the first 20 μs after the laser pulse was fired. A Gaussian temperature distribution reflecting the laser energy distribution with a maximum temperature of 800 K and a flat gas density distribution at 15 mbar were assumed as initial conditions. After a few microseconds a gas density bubble is formed while a pressure wave is expanding radially with a velocity of around 0.6 $mm/\mu s$ (figure 6). At 15 μs the density on axis has droped by 70 percent.

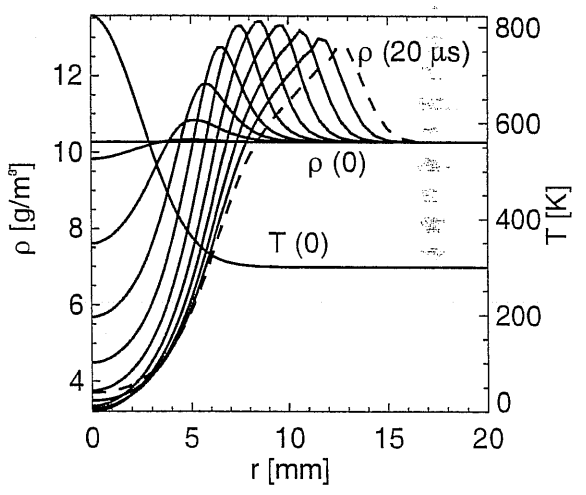

FIG. 6. Hydrodynamics of the laser heated gas as calculated by CYCLOPS. The graph shows the temporal evolution of the gas density profile during the first 20 μs in 2 μs steps as well as the initial temperature profile after the laser heating near the anode.

Figure 7 shows the temporal evolution of the gas density on axis for different initial temperatures of the laser heated gas at a pressure of 15 mbar. For 500 K the gas density drops by 40 percent within the first 15 μs, for 1800 K by 80 percent. A minimum gas density is reached at 15 μs. After this time the density increases again by a few percent until it reaches a steady state at around

20 μs with a very small increase for the next hundreds of microseconds. The same behaviour can be observed for different initial gas pressures. The size of the density bubble does not depend on the maximum initial temperature but only on the shape of the laser footprint.

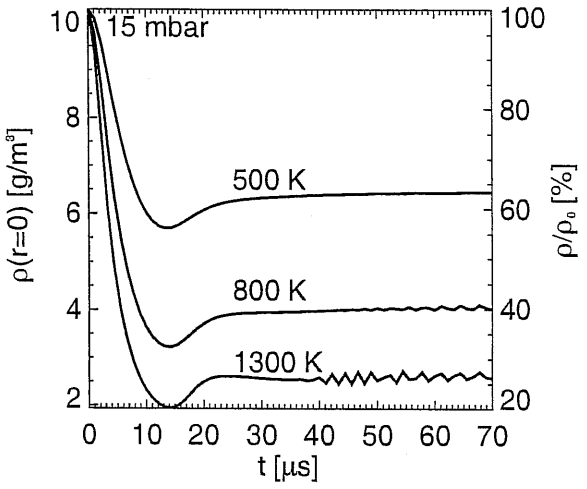

FIG. 7. Evolution of the gas density on axis for three different initial gas temperatures.

The time where the minimum gas density is reached depends only on the width of the initial temperature profile but not on the gas pressure or the maximum temperature. For gaussian profiles the width and the time of the minimum scale linearly for widths of a few mm to cm as used in the experiment.

The evolution of the rarefaction channel manifests itself indirectly in the discharge delay (figure 8). For a voltage close to the breakdown limit (dashed curve in figure 5) the discharge ignites after a certain delay depending on voltage, pressure and the laser pulse characteristics.

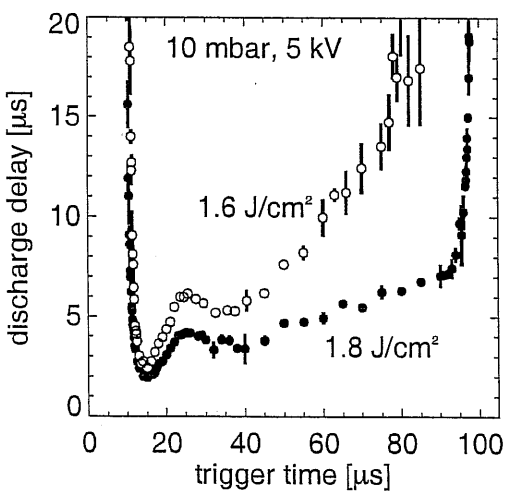

FIG. 8. Discharge delay at different discharge trigger times with respect to the laser heating.

The jitter of this delay is in the order of tens of ns for delays of up to few μs. As the pressure exceeds the critical value, the delay increases fast in the tens of microseconds range (figure 9). In this regime, the jitter in the order of tens of μs does not allow reproducible discharge conditions. For even higher pressures no channel can be created. Already during this delay a very weak channel self emission can be recorded with an image intensified camera. While at this time the gas pressure is still too high for an electron avalanche a small current is driven through the rarified gas, causing additional joule heating and gas rarefaction.

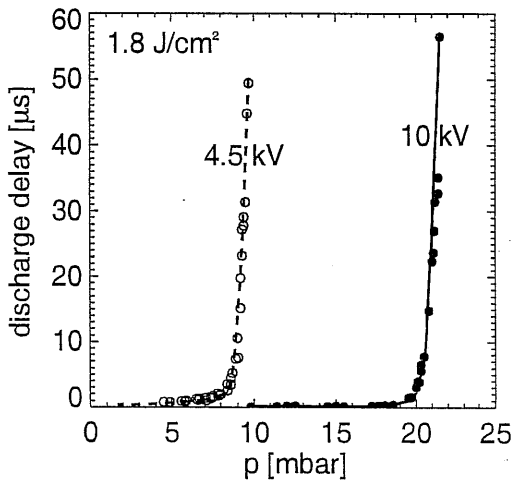

FIG. 9. Discharge delay as a function of pressure for 4.5 kV and 10 kV. The graph shows the sudden increase of the delay as the pressure exceeds a critical value.

The minimum discharge delay is obtained for the discharge beeing triggered 15 μs after the laser pulse. This minimum and the subsequent increase by a few percent is in very good agreement with the hydro-simulation, indicating that the discharge delay is determined primarily by the gas density.

With a *pd* product in this experiment of around $2 \cdot 10^2$ $torr \cdot cm$ the discharge behaviour is characterized by the linear right-hand branch of the room temperature Paschen curve [18]. A density reduction of 70 percent should cause a similar reduction of breakdown voltage. Olsen [17] showed that the breakdown behaviour can only be explained by a combined effect of high temperature and rarified gas.

V. CHANNEL STABILITY AND EVOLUTION

A series of photographs of a 44 kA main discharge in 10 mbar recorded side-on with a gated, image intensified camera with an exposure time of 100 ns is shown in figure 10. The discharge was fired 15 μs after the laser pulse. The pictures show reproducibly straight, stable channels,

even after the current maximum reached at 4 μs.

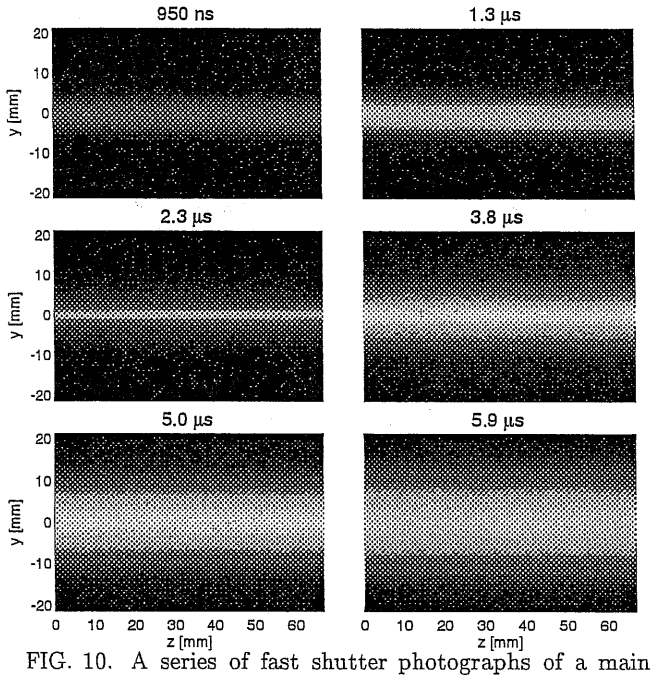

FIG. 10. A series of fast shutter photographs of a main discharge in 10 mbar taken at different times.

Due to the size of the vacuum windows, only the central section of the channels with a length of 70 mm is visible. Straight channels could be produced up to pressures of more than 20 mbar for early times before the current maximum. However above 15 mbar the channels show instabilities mainly of the kink type at times later than 3 to 4 μs. A lower pressure limit is set by the decreasing absorption and the onset of insulator breakdown. Straight, stable channels were created at pressures as low as 2 mbar. Prepulse discharges with 1 kA and main discharges with reduced bank capacity at 20 kA are stable throughout the entire investigated pressure range from 2 to 25 mbar. Stable discharges were also produced with a preceeding prepulse channel triggered 10 μs before the main bank and 15 μs after the laser pulse, up to pressures of 20 mbar. A delay bigger than 20 μs between prepulse and main discharge creates stable channels only during the first 3 to 4 μs.

The channel evolution for different discharge conditions measured by streak and fast shutter imaging is shown in figures 11 and 12. Channel diameters were determined as the FWHM of a Gauss fit to the profiles obtained from the fast shutter images. Discharges at 15 mbar (figure 12) show a pinching from a diameter bigger than 10 mm down to 3 mm at around 1.2 μs. Discharges at 5 mbar show a second less pronounced pinch at the time of the current maximum around 4 μs. Different laser energy deposition or discharge trigger delays do not show any difference in the channel diameter within the range of accuracy.

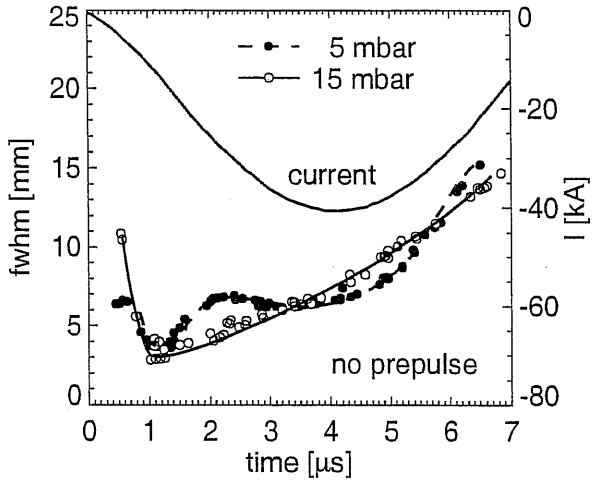

FIG. 11. Channel evolution and discharge current for a discharge at 5 mbar and 15 mbar without prepulse discharge.

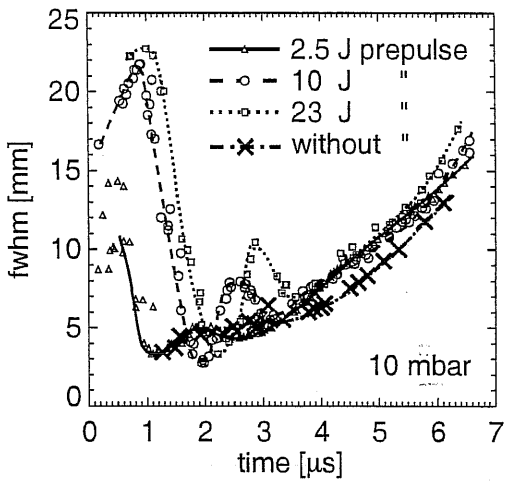

FIG. 12. Channel evolution for a main discharge at 10 mbar with 2.5 J, 10 J, 23 J prepulse and without any prepulse.

Firing the prepulse discharge prior to channel creation has a bigger effect on the channel evolution. Figure 12 shows the channel diameter evolution for a 10 mbar discharge without prepulse as well as with prepulse at different voltages. The initial conditions of the main discharge are altered considerably by the prepulse. The channel starts at larger initial diameters compared to discharges without prepulse, indicating a lower initial pressure on axis caused by the prepulse. Subsequently the discharge pinches down to around 3 mm at a time of 1.1 μs, 2.0 μs and 2.3 μs for a prepulse energy of 2.5 J, 10 J and 23 J respectively. In all three cases a second less pronounced pinch occurs at 2.6 μs, 3.3 μs and 3.5 μs like in the 5 mbar discharge without prepulse. After the current maximum the channel expands with a radial velocity of around 1 $mm/\mu s$ independent of the predischarge.

VI. CONCLUSION AND OUTLOOK

The channels fullfill the requirements for ion beam transport. They are straight, stable and reproducible up to the current maximum. The jitter is small compared to the discharge evolution timescale. Breakdown along the wall was not an issue within thousands of discharges. First experiments to study the ion optical properties of such channels have been performed at the UNILAC linear accelerator at GSI [11]. In this first run C^{2+} ions with an energy of 13.5 AMeV were transported with high efficiency over a quarter of a betatron oscillation. At that time a different laser with lower energy and a much stronger variation of the laser spot size troughout the chamber produced only unstable channels. Recently, additional runs on the stable channels described here were performed with ion beams of different species, where more than a full betatron oscillation was observed. This results as well as advanced channel diagnostics such as imaging interferometry, spectroscopy and magnetic field measurements will be reported in following companion papers.

ACKNOWLEDGMENT

This work is supported by the German BMBF.

---

[1] J.R. Freeman, L. Baker, D.L. Cook, 'Plasma Channels for intense Light-Ion-Beam Transport', Nucl. Fus. **22**, 383 (1982)

[2] J.N. Olsen et al., 'Ion beam transport in laser-initiated discharge channels', J.Appl.Phys. **53**(5), 3397 (1982)

[3] P.F. Ottinger et al., 'Z-discharge transport of intense ion beams for inertial confinement fusion', J. Appl. Phys. **70**(10), 5292 (1991)

[4] F.A. Sandel et al., 'Experimental Studies of Intense Light-Ion Beam Transport', Proc. 4th Int. Conf. on High-Power Electron- and Ion Beams, Palaiseau, France 129-136 (1981)

[5] J. Neri et al., 'Intense ion-beam-transport experiments using a z-discharge plasma channel', Phys. Fluids B5, 176-189 (1993)

[6] J.N. Olsen et al., 'Propagation of light ions in a plasma channel', Appl. Phys. Lett. **36**, 808-810 (1980)

[7] T. Ozaki et al., 'Light ion beam transport in a multi-plasma channel system', Proc. 5th Int. Conf. on High-Power Part. Beams, San Francisco, 78-81 (1983)

[8] A. Tauschwitz et al., 'Plasma lens focusing and plasma channel transport for heavy ion fusion', Fus.Eng.Des. **32-33**, 493-502 (1996)

[9] S. Yu et al., 'Plasma-channel-based reactor and final transport', Nucl. Instr. and Meth. A **415**, 174-181 (1998)

[10] M.C. Vella, T.J. Fessenden, W. Leemans, S. Yu, A. Tauschwitz, 'Plasma pinch for final focus and transport', Nucl. Instr. and Meth. A **415**, 193-199 (1998)

[11] A. Tauschwitz et al., 'Ion Beam Transport in a Laser Initiated Discharge channel', Proceedings: Inertial Fusion Sciences and Applications 1999, Editors: C. Labaune, W. Hogan, K. Tanaka, Elsevier, 521-526 (1999)

[12] J.N. Olsen, 'Laser-initiated channels for ion transport: CO_2-laser absorption and heating of NH_3 and C_2H_4 gases', J.Appl.Phys. **52**(5), 3279 (1981)

[13] W.M. Manheimer et al., Phys. Fluids **16**, 7, 1126 (1973)

[14] E. Henestroza, S.S Yu, M.C. Vella, W.M. Sharp, 'Simulations of channel-based final beam transport', Nucl. Instr. and Meth. A **415**, 186-192 (1998)

[15] K. Vandersloot, HIFAR 500, LBNL report 46692 (2000)

[16] D.M. Ponce et al., 'Diagnostics of plasma channels for HIF transport', to be published in Nucl. Instr. and Meth. A (2001)

[17] J.N. Olsen et al., 'Laser-initiated channels for ion transport: Breakdown and channel evolution', J.Appl.Phys. **52**(5), 3286 (1981)

[18] H.E. Radford, 'Electrical breakdown in ammonia at low pressure', NBS report 9882, 1968